Digital light processing stereolithography of zirconia ceramics: Slurry elaboration and orientation-reliant mechanical properties

Digital Light Processing stereolithography of zirconia ceramics: slurry elaboration and orientation-reliant mechanical properties

Bartolomeo Coppola[1,*], Julien Schmitt[2], Tanguy Lacondemine[2],Caroline Tardivat[2], Laura Montanaro[1] and Paola Palmero[1]

[1] Politecnico di Torino, Department of Applied Science and Technology, INSTM R.U. Lince Laboratory, Corso Duca Degli Abruzzi, 24, Italy

[2] LSFC Laboratoire de Synthèse et Fonctionnalisation des céramiques UMR 3080 CNRS / Saint-Gobain CREE, Saint-Gobain Research Provence, 550 avenue Alphonse Jauffret, Cavaillon, France

Abstract

Digital Light Processing (DLP) is a promising technique for the preparation of ceramic parts with complex shapes and high accuracy. In this study, 3 mol% yttria-stabilized tetragonal zirconia polycrystal (Y-TZP) UV-curable slurries were prepared and printed via DLP. Two different solid loadings (40.5 and 43.6 vol%, respectively) and printing directions were investigated to assess the influence of these parameters on physical and mechanical properties of the sintered parts. Zirconia samples were sintered at 1550 °C for 1h, achieving a very high relative density (99.2 %TD), regardless of solid loading and printing direction. FE-SEM micrographs shown a homogeneous and defect-free cross section with an average grains size of 0.56 ± 0.19 μm. Finally, mechanical properties were influenced by printing direction and zirconia vol%. Indeed, the composition with the higher solid loading (i.e. 43.6 vol%) had the highest three-point flexural strength (751 ± 83 MPa) when tested perpendicular to the printing plane.

Keywords: Stereolithography, Digital Light Processing; 3D printing; Zirconia; Microstructure; Mechanical properties

1. Introduction

3D printing technologies, also known as additive manufacturing processes, allow to shape materials behind the current limits, by expanding the design freedom and improving the process speed while reducing cost and waste. Although the implementation of 3D printing technologies in the ceramic industry has been slower compared to the polymer and metal fields, the disruptive potential to apply these technologies to technical ceramics has been fully recognized. In spite different 3D printing processes are nowadays available [**1**], stereolithography (SLA) offers advantages in terms of printing resolution and precision, which – beside the high quality of surface finishing - make it the most proper additive manufacturing technology for engineering ceramics. The SLA technology is based on the layer-by-layer polymerization of a photocurable liquid monomer, filled with ceramic particles; in particular, it employs a UV laser beam which moves from point to point tracing the photopolymerized geometry. The Digital Light Processing (DLP) is a different type of SLA, where the light source is a UV projector, able to cure a complete layer of resin at a time, enhancing the process speediness. Among technical ceramics, 3D-printed zirconia is gaining increasing interest, due to the different application fields in which this material can be used [**2**]: for dental implants and frameworks [**3,4**], as electrolyte [**5,6**] and monolithic support for solid oxide fuel cells [**7**], as part for cutting blades and tools [**8**], for complex-shaped molds [**9**] and other precision parts for mechanical and thermal applications [**10**]. The challenge is the fabrication of defect-free, fully dense ceramics, with properties comparable to those of materials processed by conventional technologies. This requires the control of many processing steps: from the preparation of the slurry, to the optimization of the printing parameters, the set-up of suitable debinding and sintering thermal cycles. However, even if SLA and DLP are mature technologies for zirconia 3D-printing, most of the papers focus mainly on the slurries preparation [**11-14**], and just a limited number also explores the mechanical properties of the final materials [**15-17**]. Concerning the optimization of the process of 3Y-TZP slurries preparation, and in particular on the role of solid loading, dispersants and rheological behavior, some key contributions were provided by the following works. Li et al. [**11**], investigated the role of dispersant in tailoring the viscosity of zirconia slurries preparation. Authors optimized the dispersant (Disperbyk-103) amount and found that 3.5wt% was the optimal concentration to give a high solid loading (42 vol%) zirconia photocurable dispersion, with a low viscosity (<5 Pa·s at 30 s^{-1} shear rate) and a representative shear-thinning behavior suitable for stereolithography applications. Sun et al. [**12**] investigated

the preparation of a very high solid content slurry (83 wt%), by optimizing the Disperbyk concentration at 5wt%. Rheological and UV-Vis transmittance tests demonstrated that lower dispersant amounts were not sufficient to counteract the Van der Waals forces, and thus the slurry dispersibility was poor and the viscosity high. At the optimum amount, the correct steric hindrance effect of the dispersant was achieved: the slurry became homogeneous and stable, with a low viscosity (1.48 Pa·s at 50 s^{-1} shear rate). At higher amount, the excess of dispersant molecules in the slurry caused flocculation, and promoted a slight increase of the viscosity. Zhang et al. [**13**] tested a wide number of compositions using three dispersant types, several dispersant concentrations (0.5, 1, 2, 3, 4 and 5 wt%) and solid loadings (30, 40, 50, 55 and 60 vol%). Similarly to the previous research, the Authors determined an optimum dispersant amount at 2 wt% for 40 vol% solid loading slurries, as lower dispersant concentration was not enough to provide suitable viscosity, while higher concentration caused flocculation of the slurry.

Concerning the role of the slurry parameters on the mechanical properties, references [**15,16**] provide the current main contributions. Borlaf et al. [**15**] investigated different solid loadings (41, 44 and 47 vol%), deepening the study on the intermediate concentration, and achieving an average four-point bending strength of 740 MPa. Jang et al. [**16**] investigated different solid loadings (ranging between 48-58 vol%) for the preparation of zirconia slurries, and observed a progressive increase of the flexural strength by increasing the solid loading. In addition, fewer cracks and interlayer flaws were present in the materials at the highest ceramic fractions. Further papers dealt with the characterization of the mechanical strength of DLP-printed zirconia ceramics [**10,18**], and few papers explored the role of printing orientation on the mechanical properties [**19,20**], but in such previous works the slurry preparation and its role on the final properties was not investigated. Therefore, the aim of this work is to provide a general overview of the main parameters able to affect the mechanical properties of zirconia ceramics fabricated by DLP. Thus, the preparation of printable zirconia slurries was optimized and the influence of solid loading and printing direction on the mechanical properties were investigated. Samples were submitted to flexural strength characterization, by testing them in the as-sintered state (i.e., without any further steps of polishing or machining), whit the aim to prove the ability of the DLP process to fabricate high-quality surfaces, as a key advantage over the other traditional as well as 3D printing technologies.

2. Material and methods

2.1. Materials

A 3 mol% yttria-stabilized zirconia powder (CY3Z, Saint-Gobain ZirPro) was used as starting material. **Figure 1a** shows the particle size distribution of CY3Z powder, characterized by a monomodal and narrow distribution which ranges from about 0.1 to 2 μm, with a d_{50} of approx. 0.50 μm. In **Figure 1b**, it is possible to observe that the powder forms small agglomerates made by ultrafine primary particles, whose size ranges from about 100 to 250 nm. Let us note that the technical data sheet for CY3Z mentions a d_{50} of ca. 0.2-0.3 μm and a specific surface area (SSA) of 7 m^2/g [**21**]. The slightly higher value found here could be related to a lower degree of de-agglomeration of the particles before size analysis.

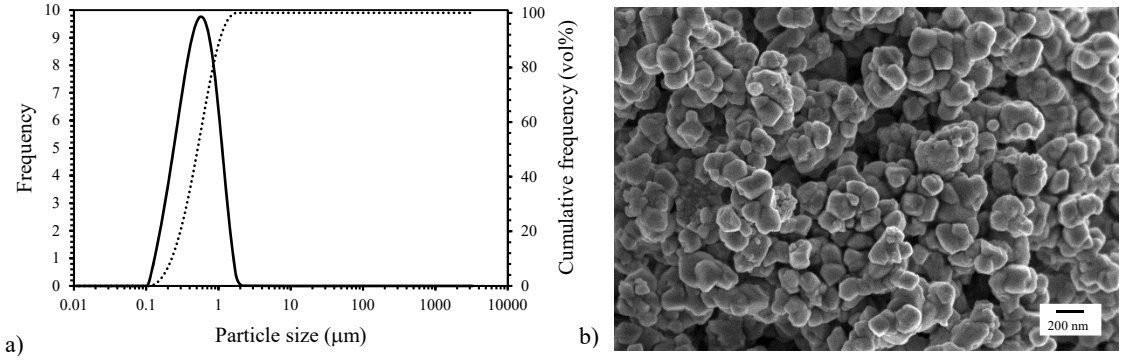

Figure 1: a) particle size distribution and b) FE-SEM micrograph of CY3Z powder

The slurries were prepared by mixing suitable amounts of CY3Z with a commercial photocurable resin (ADMATEC Europe BV, The Netherlands). To achieve a high solid content and a satisfactory viscosity, a commercial dispersant (Disperbyk-103, BYK Chemie, Germany) was used as well. Slurries were prepared in three steps: i) photocurable resin and dispersant were firstly mechanically mixed for few minutes at room temperature; ii) then, the zirconia powder was gradually added to the resin and dispersant solution, and stirred for approx. thirty minutes; iii) finally, the slurry was poured in agate jars with agate spheres (d = 5 mm) and milled for 3 hours at 350 rpm in a planetary miller (Fritsch Pulverisette, Fritsch GmbH, Germany). Slurries at two different solid loadings were prepared (79 wt% and 81 wt%, which correspond to 40.5 vol% and 43.6 vol%, respectively), using in both cases 1 wt% of dispersant respect to the zirconia powder.

2.2. Digital Light Processing (DLP) and post-processing

Two types of prismatic samples were designed using the AutoCAD software. A first set of samples was designed for dilatometric analysis (final dimensions of approx. 20 x 3 x 4 mm), while longer samples were designed for three-point bending tests (final dimensions of 32 x 3 x 4 mm). Specimens were printed using a DLP-based stereolithographic device (ADMAFLEX 130, ADMATEC Europe BV, The Netherlands). The main printing parameters were optimised to achieve a good quality printing, following our previous works [**22**]. Thus, layer thickness, exposure time and LED power were fixed at 30 µm, 1000 ms and 250 ‰, respectively. To understand the influence of printing orientation on the physical and mechanical properties of the sintered samples, two different printing orientations were investigated (**Figure 2a**). In the first case, samples were printed vertically on the printing plane (samples labelled XZ), while in the second, the samples lied on the printing plane (samples XY), as shown in **Figure 2b**. This means that the XZ samples were built by 133 layers and the XY ones by only 100 layers. 10 samples for each slurry solid loading and printing orientation were produced, for a total of 40 samples.

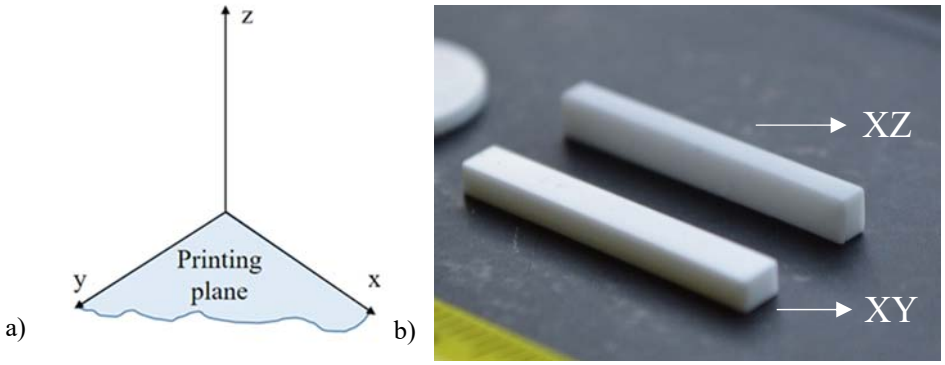

Figure 2: a) schematic representation of the printing plane and b) sintered samples (at 1550 °C for 1h) printed in the two directions

After printing, samples were soaked in deionized water at approx. 40 °C for 24 h to remove uncured slurry. Then, samples were oven dried at 70 °C for 6 h and finally submitted to a thermal debinding and sintering (Carbolite 1800 electric furnace, Carbolite Gero GmbH) cycle, depicted in **Figure 3**. In particular, samples were slowly heated up to 1000 °C to avoid cracking during resin decomposition and then sintered up to 1550 °C (heating rate 1 °C/min) for 1 h. This sintering temperature was chosen on the ground of dilatometric

analyses, as discussed in the following. The sintered density was calculated according to the theoretical density (TD) of 3Y-TZP (6.05 g/cm^3).

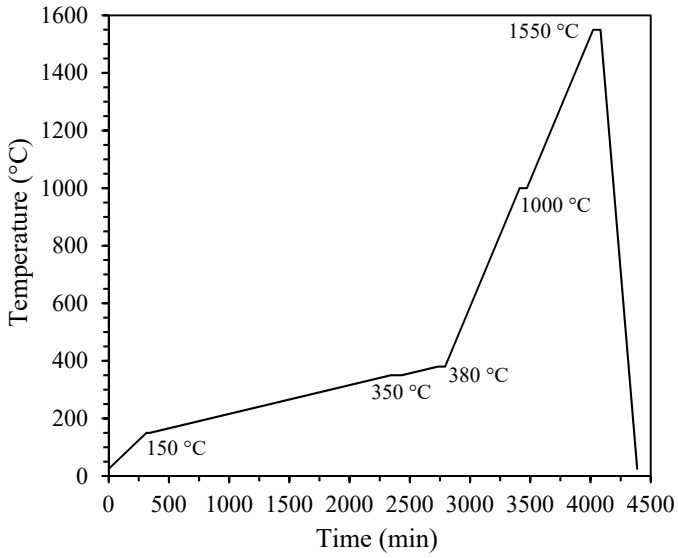

Figure 3: Thermal debinding and sintering program

2.3. Characterization

Slurries rheological behaviour was investigated using a rotational rheometer (Kinexus Pro+, Netzsch Geraetebau GmbH, Selb, Germany) equipped with stainless steel roughened parallel plates (20 mm diameter) with a 1 mm gap between plates. For comparison, slurries with the same solid loading but without dispersant were prepared and characterized, too. The densification behaviour was investigated by dilatometric analyses (Netzsch 402E, Germany), carried out up to 1550 °C for 1 h, using the same thermal program reported in **Figure 3**. The fired density, ρ (g/cm^3), was determined via buoyancy method, following Archimedes' principle (Density Determination Kit, Sartorius YDK01). Ceramic parts microstructures were investigated by means of a FE-SEM (FESEM Hitachi S4000) on polished and thermally etched surfaces. Grain size and their statistical distribution were determined by image analysis (Scandium Soft imaging system software) measuring at least 200 grains. XRD analysis was performed both on the raw powder and sintered samples using a Pan'Analytical X'Pert Pro instrument (Pan'Analytical, Almelo, The Netherlands) with CuKα radiation (0.154056 nm) in the 2θ range 25-65°. To determine the volume of monoclinic phase, the intensities of the monoclinic (-111) and (111) peaks and of the (101) tetragonal peak were integrated, according to the Garvie

Nicholson method [**23**]. Phases were identified by JCPD file n. 00-037-1484 and n. 01-083-0113 for monoclinic and tetragonal zirconia, respectively.

Hardness was measured by means of Vickers indentation (MicroMet 6000 Series Buehler) after surface polishing down to 1 µm. A series of 10 indentations were performed on each material with an applied load of 200 g_f, with a 15 s dwell time. The hardness was calculated from the applied load, previously selected to avoid cracks, and the two diagonals length of the indent (**Figure 4**), according to the standard equation [**24**]. Hardness was measured on the external surface parallel to the printing plane and on the surface perpendicular to the printing plane.

Samples flexural strength was determined by 3 points bending tests using a Shimadzu AGSX traction/compression machine. Eight samples of dimensions 25 x 2 x 3 mm (L x W x H) were tested with a crosshead speed of 100 µm/s and a support span of 18 mm. The load was measured thanks to a 10 kN force sensor and the sample deflection, under the loading pin, was measured during testing thanks to a Linear Variable Differential Transformer (LVDT) sensor. The Young's Modulus of the different materials was estimated from the linear slope of the load-displacement curves.

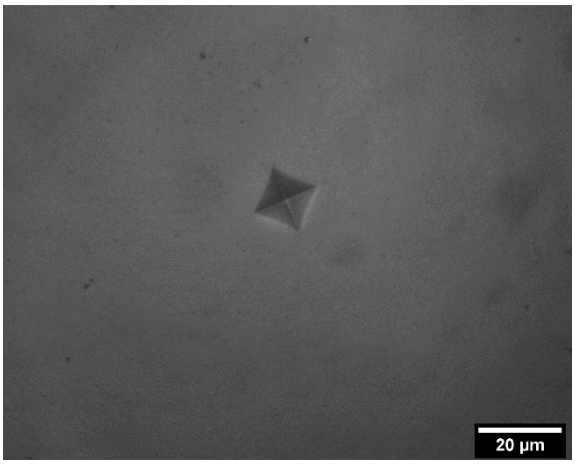

Figure 4: Example of Vickers indentation for Hardness (test load of 200 g_f) measurement, here for the composition 79 wt%

3. Results and discussion

3.1. Rheological behavior

Slurries printability was evaluated through rheological measurements and the results are reported in **Figure 5**. All the slurries display a shear-thinning behaviour in the investigated shear rates range (**Figure 5a**). Moreover, the effect of the dispersant in reducing slurries viscosity can be clearly observed. Indeed, at low shear rates (for instance, at 0.1 s^{-1}), slurries without dispersant showed a viscosity two (79 wt%) or three (81 wt%) orders of magnitude higher than the slurries at the same solid loading but containing 1 wt% of dispersant. Furthermore, at shear rates between 100 and 200 s^{-1} (i.e. those used during 3D-printing, see **Figure 5b**), 1 wt% of dispersant was enough to reduce handcraft slurries viscosity at values between 2 and 4 Pa·s, and thus below the maximum viscosity value (i.e. 5 Pa·s) proposed by Licciulli et al. [**25**] to achieve good printability. These results confirm the good affinity between DISPERBYK-103 and zirconia powder as previously reported in the literature [**11**].

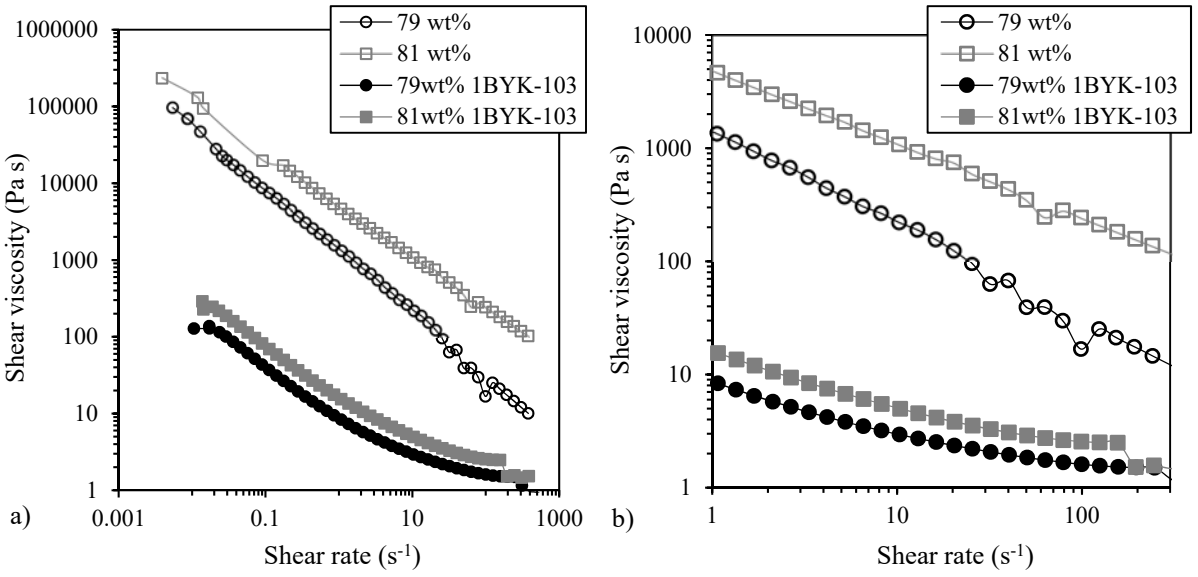

Figure 5: Effect of dispersant on the rheological behaviour of the investigated compositions: a) entire range of tested shear rates and b) enlargement of the range 1-300 s^{-1}

3.2. Dilatometric tests

Green samples produced by stereolithography were characterized by geometrical density, and values are collected in **Table 1**. Samples of the same geometry (bars of 3 x 4 x 20 mm) but printed along XY and XZ directions showed almost the same values, suggesting that the layers' number did not affect the green density. On the opposite, a certain role of the solid loading was observed, with an expected higher density of the 81 wt% formulation compared to the 79 wt% one.

Thus, one representative sample from the 79 wt% and 81 wt% batches – regardless the printing direction - was submitted to dilatometric analysis. It was in fact considered that the samples exhibit the same linear contraction in the plane (i.e. in the X and Y direction) while they could differ only on the Z-axis, which is however not measured by the dilatometry.

Table 1: green and sintered density, shrinkage in the X and Z directions for bars derived by slurries at 79 wt% and 81wt% solid loading, and printed along the XY and XZ directions.

Solid loading	Printing Direction	Green density (% TD)	X-axis shrinkage (%)*	Z-axis shrinkage (%)**	Sintered density (g/cm^3)
79 wt%	XY	42.3 ± 0.2	24.2 ± 0.1	24.8 ± 0.3	6.00 ± 0.03
	XZ	42.2 ± 0.4	24.2 ± 0.1	25.0 ± 0.1	6.01 ± 0.01
81 wt%	XY	45.0 ± 0.8	22.3 ± 0.2	23.1 ± 0.4	6.01 ± 0.01
	XZ	45.1 ± 0.4	22.3 ± 0.2	23.8 ± 0.3	6.00 ± 0.02

*by dilatometric analysis; **by precision calibre

Linear shrinkage of the samples during either debinding and sintering processes are reported in **Figure 6**. For both compositions, a small expansion (approx. 0.35%) up to 150 °C is visible, while samples exhibit a ca. 1% shrinkage between 150 °C and 400 °C, due to the removal of the polymeric resin. The small step at 1000 °C, which is visible in both densification and derivative curves, is imputable to the short isothermal stage performed at that temperature, before the start of the high-temperature sintering cycle (**Figure 3**). From both densification and derivative curves, no meaningful differences in terms of onset sintering temperature and maximum sintering rate temperature (T_{onset} and T_{max}, respectively, this latter identified by the peak of the derivative curve) can be detected. The samples at the two solid loadings showed almost superimposable linear shrinkage till T_{max}, then the 79 wt% formulation underwent a higher shrinkage till the maximum

heating temperature (1550 °C). The 79 wt% and 81 wt% samples reached total linear shrinkages of -24.2% and – 22.3%, respectively (**Table 1**). As expected, linear shrinkages in the Y-direction (as measured by a precision calibre) are comparable to the X-ones, while a certain difference is observed in the Z-axis. Indeed, samples made using the 79 wt% formulation exhibit a Z-axis shrinkage that is 2.5% higher than in the X-axis when printed in the XY direction; while the increase reaches 3.5% for the XZ direction, as it was built through a larger number of layers. A similar trend is observed for samples made at 81 wt%, with an increase of the Z-axis shrinkage of 3.4% and 6.3% for the XY and XZ-printed bars respectively. The anisotropic shrinkage in stereolithography printed materials, and particularly the highest contraction along the Z-axis, has been already documented in the literature [**17**] and is associated to a non perfect packing ability of the layers in the vertical direction [**20,26**]. In spite these differences in shrinkages, the final sintered materials reached the same fired density (> 99.0 %TD), as indicated in Table 1.

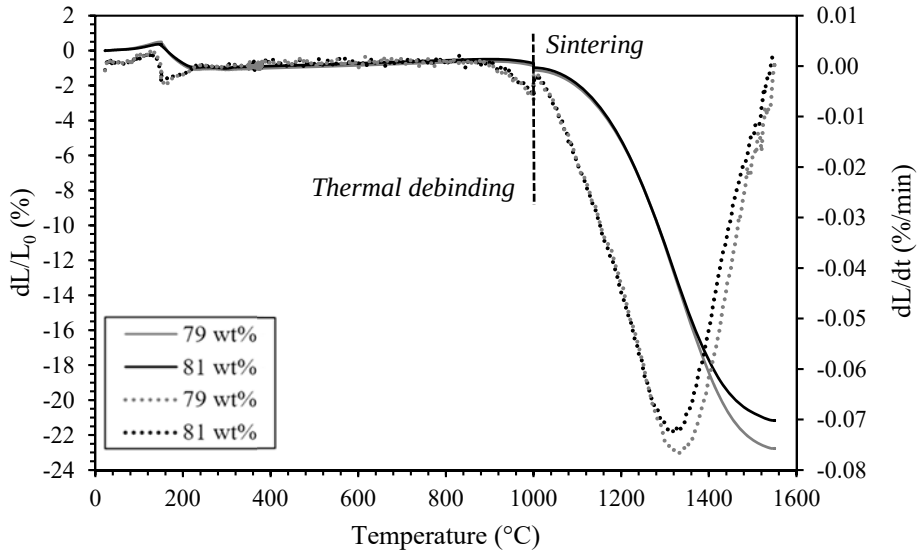

Figure 6: Dilatometric (solid lines) and derivative (dotted lines) curves of 79 and 81 wt% samples heated up to 1550 °C for 1 h

3.3. Phase composition and microstructure

Crystalline phases present in the as-received powder and sintered samples were identified using XRD analysis and the patterns are reported in **Figure 7**. All the patterns present the characteristic peaks of monoclinic (00-037-1484) and/or tetragonal (00-048-0224) zirconia. The monoclinic content in the as-received powder is 48% while no monoclinic zirconia is detected in the sintered sample (being completely tetragonal).

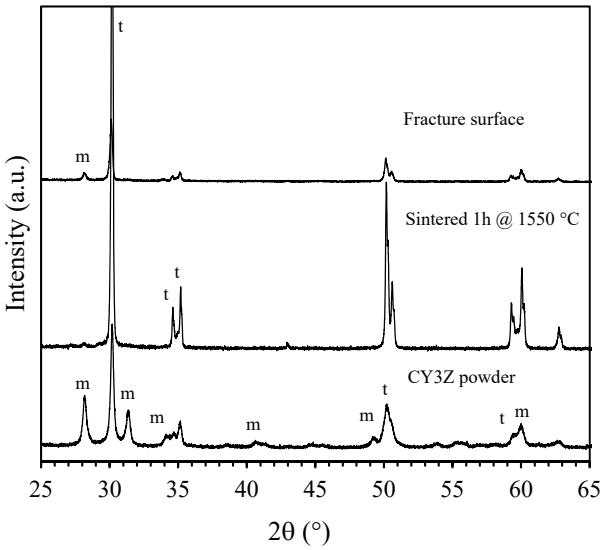

Figure 7: XRD patterns corresponding to CY3Z powder (as received); 81 wt% sample sintered 1h @ 1550 °C and fracture surface of a 81 wt% sample sintered 1h @ 1550 °C

In order to evidence possible printing defects as well as to observe the green and sintered microstructures, some representative samples were submitted to FE-SEM characterization. In **Figure 8a**, the FE-SEM micrograph of an as-printed 79 wt% sample carried out on the fracture surface is depicted, showing a homogeneous and highly compact microstructure, almost free from large printing defects. The printing layer can be easily observed, showing an average thickness of 27.3 ± 0.9 μm. Considering that the nominal layer thickness was 30 μm, this average value and its standard deviation highlight the high precision and accuracy of the printing process. At higher magnification (**Figure 8b**), we can observe a homogeneous microstructure made by ultrafine particles, with printing layers free from pores or other large interlayer flaws. After sintering, a still homogeneous and dense microstructure can be observed. The low-magnification fracture

surface (**Figure 8c**) shows a compact material with a defect-free structure. At higher magnifications, **Figure 8d**, it is possible to distinguish again the printed layers (red dotted lines), whose average thickness was 22.2 ± 0.9 μm, this value being in a very good agreement with the expected one, considering the imposed layer thickness (30 μm) and the Z-axis shrinkage during sintering (25%).

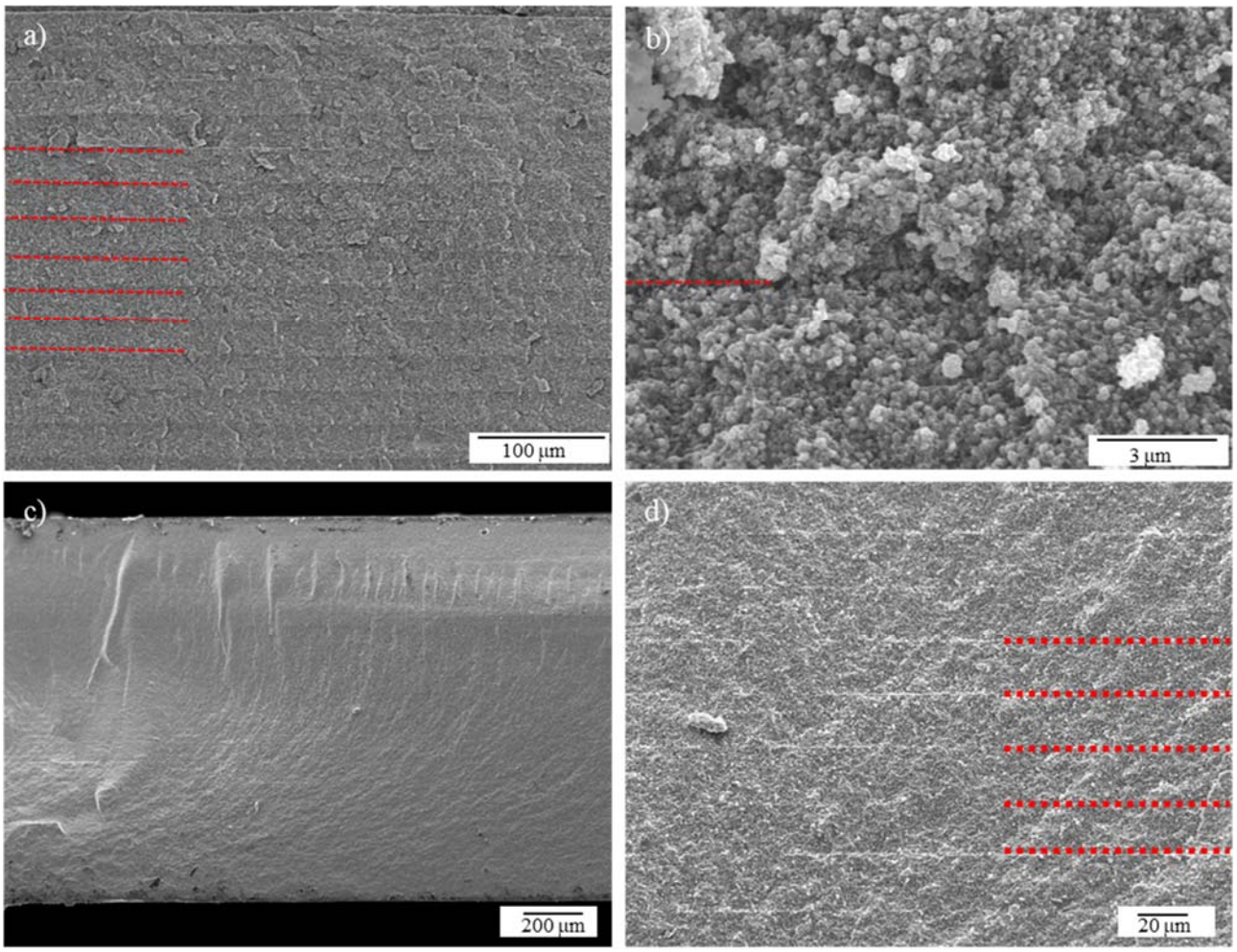

Figure 8: FE-SEM micrographs of as-printed (a,b) and sintered (c,d) samples, produced from the 79 wt% slurry; lower (a, c) and higher (b,d) magnification fracture surfaces (layers are highlighted with red dotted lines)

The microstructure of a sintered sample (still at 79 wt% solid loading) after polishing and thermal etching is shown in **Figure 9**. As already observed for the cross section, the low-magnification image of the polished surface (**Figure 9a**) also shows a very homogeneous and defect-free microstructure, attesting the correct choice of the slurry characteristics and printing parameters. Higher magnifications micrographs (**Figure 9b-c**) reveal the typical fine-grained microstructure of yttria-stabilized zirconia, and highlight a fully densified microstructure. Thus, the lack of evident printing flaws as well as the fully dense microstructure observed,

validate the very high relative density obtained (99.2 %TD). Finally, the highest magnification micrograph (**Figure 9d**) shows the quite wide dimensional range of zirconia grains, as some ultra-fine grains (in the nanometric range) are visible among submicrometric ones.

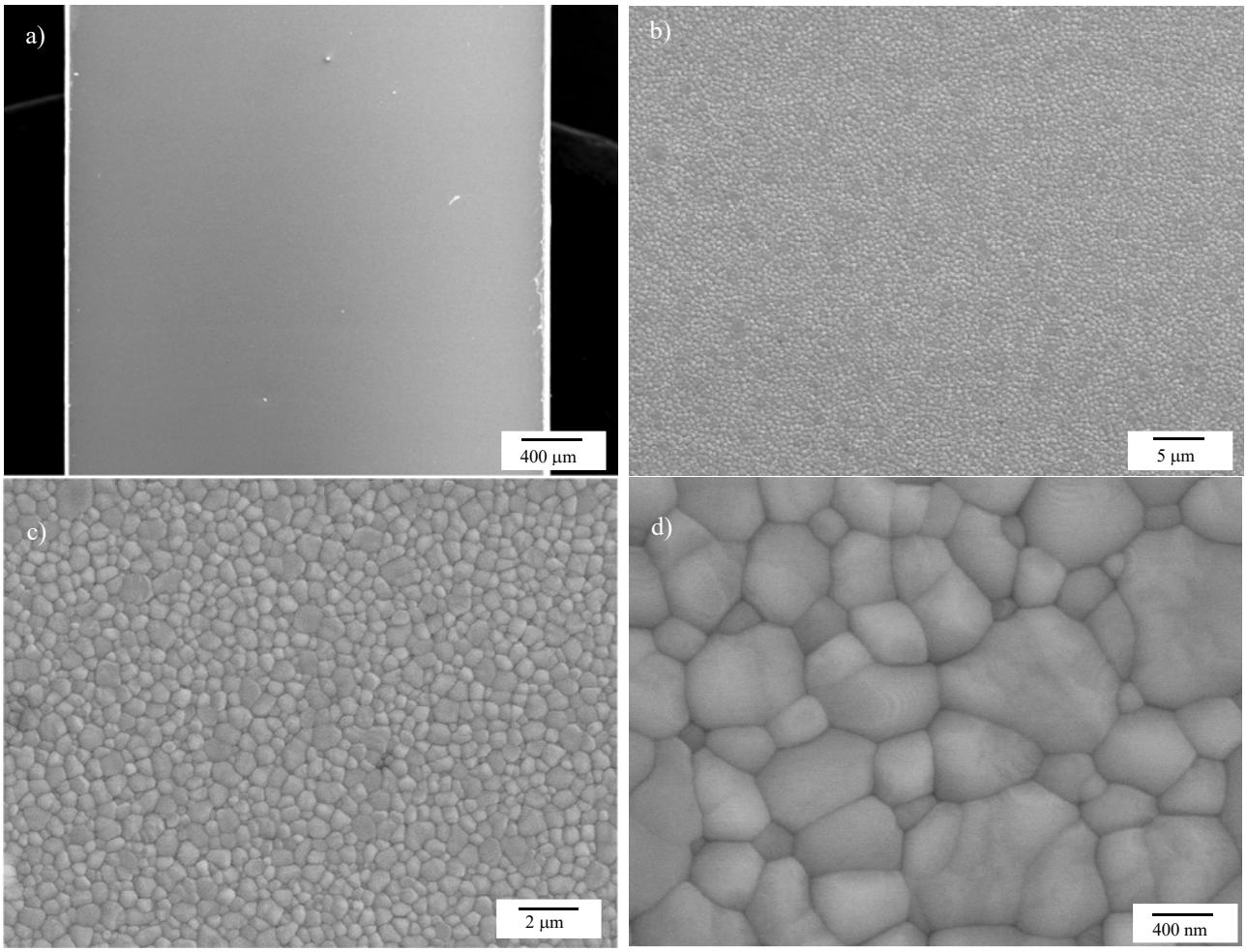

Figure 9: FE-SEM micrographs, at increasing magnifications from a) to d), of a polished surface of a 79 wt% sample

Very similar microstructural features (including green and sintered samples) were observed for the 81 wt% formulation. Image analyses performed on the sintered microstructures, revealed a similar average grain size and similar grain size distribution (**Figure 10**), regardless slurry solid loading and printing direction. As mentioned before, zirconia grains fall within a certain dimensional range with the majority of the grains in the range 0.40-0.60 µm. In particular, the average grain size for 81 wt% composition was 0.55 ± 0.19 µm while for 79 wt% composition was 0.57 ± 0.19 µm.

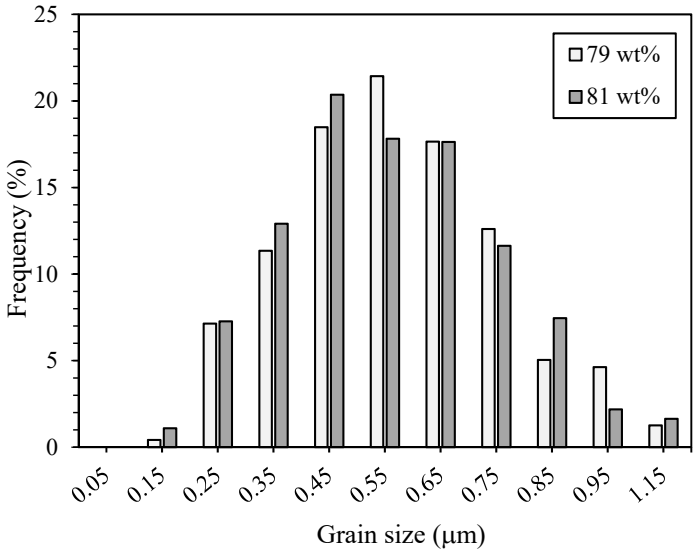

Figure 10: Grain size distribution for 79 wt% and 81 wt% sintered samples

3.4. Mechanical properties

Flexural strength and elastic modulus were measured using three-point bending test and the results are reported in **Table 2**. For the sake of clarity, a schematic representation of the bending test configuration for the samples printed in the two directions is reported in **Figure 11**.

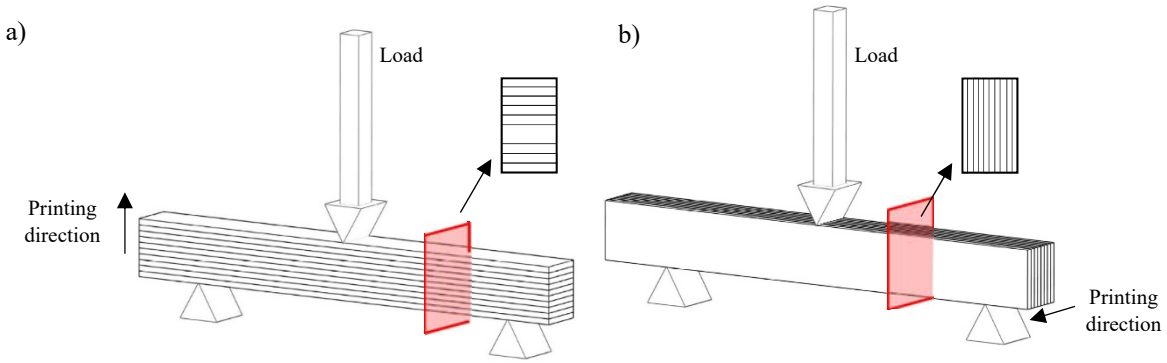

Figure 11: Schematic representation of the flexural test for a) XZ and b) XY samples

Figure 12 shows a certain dependence of the flexural strength on the solid loading and printing direction. In particular, the higher the solid loading, the higher the flexural strength. On the other side, XZ printed samples (i.e. samples tested perpendicular to the printing plane, **Figure 11**) show higher flexural strength than XY printed ones (i.e. samples tested parallel to the printing plane). Flexural strength values are in line or even higher than previous literature results on DLP-processed 3Y-TZP [**10,15,16,18,19,27**], with the highest value (751 ± 83 MPa) obtained for 81 wt% XZ samples. Wang and Dommati [**10**] determined an average strength of 731 ± 48 MPa by three-point bending test, while Borlaf et al. [**15**] determined an average value of 740 MPa (with values in the range 718 – 765 MPa). Lower values were achieved bv Jang et al. [**16**], who explored numerous slurries at different solid loadings (in the range 48-58 vol%) but achieved a maximum density of ~ 93% and maximum flexural strength of 675 MPa by 3-point-bending test. A significantly lower strength was reached by Zhang et al. [**27**] who prepared TZP ceramics by adding tetragonal zirconia particles to starting monoclinic zirconia grains. Authors determined the highest relative density and flexural strength of 96.4% and 306.5 MPa, respectively, when 7.5 vol% tetragonal zirconia was added to the monoclinic matrix. Harrer et al. [**19**] produced bars which were built by different orientations from the building platform, obtaining values strongly dependent on the printing strategy. In particular samples printed horizontally to the printing plane (as in our case) achieved a relatively low average strength of 561 MPa. A significantly higher strength (1013 MPa ± 126 MPa) was achieved by Lu et al. [**18**]; however, in this case the bars were ground and polished before testing, thus annihilating one of the advantages of stereolithography, which exploits the good finishing of the printed surfaces to avoid post-treatments.

Table 2: Summary of mechanical properties (σ, bending strength and E, Young modulus) of the ceramic parts printed in the two different directions, determined via three-point bending test

Composition	XY		XZ	
	σ (MPa)	E (GPa)	σ (MPa)	E (GPa)
79 wt%	594 ± 51	161 ± 4	706 ± 48	164 ± 5
81 wt%	675 ± 87	166 ± 14	751 ± 83	162 ± 9

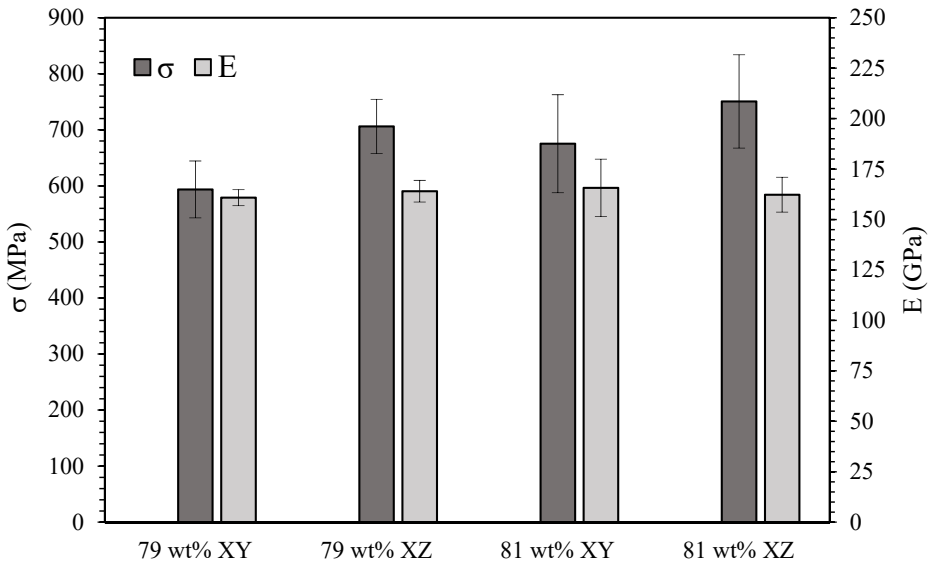

Figure 12: Variation of bending strength (σ) and Young modulus (E) as a function of solid loading and printing direction

As reported before, the XZ-printed samples showed a slightly higher mechanical strength as compared to the XY-one. This difference cannot be imputed to a different sintered density, since similar values were determined for all the bars, independently on the printing direction (**Table 1**). Since the XY and XZ bars were built by a different number of layers (100 and 133, respectively), their similar sintered density means that the layers are well packed, with limited defects between them. However, it is generally recognized that the interlayer (i.e. the contact surface between two consecutive layers) and related defects in SLA and DLP technologies provide the main contribution to failure [**20**]. Therefore, the fracture surface of the samples submitted to bending tests were further characterized by FE-SEM, as shown in **Figure 13** for the 81wt% samples. The high magnification images (b,d) show, once again, that the samples are compact, with well packed layers and almost defect-free interlayers, which cannot be associated to crack origin and propagation inside the materials. On the opposite, the lower magnification images (a,c) show that both sections are characterized by the presence of some cracks at the sample border. When the load is applied perpendicular to the printing directions, such cracks are submitted to tensile stress, and can justify the lower strength of the XY configuration.

The same images show a different roughness of the printed surface, which can be responsible of the difference in mechanical properties, too, as suggested by Fu et al. [**28**]. For the XZ samples, the surface under tension is very smooth because it was in contact with either the building platform or the printing plane and thus it could be considered almost defect free. On the contrary, for the XY samples, the surface under tension corresponds to the side of printed sample and the roughness should correspond to the consecutive printed layers. In this case, every interlayer is a potential point of stress concentration and location for easier crack initiation, thus reducing bending strength. It is worth mentioning that samples were tested after sintering without any polishing or machining step, meaning time and cost saving.

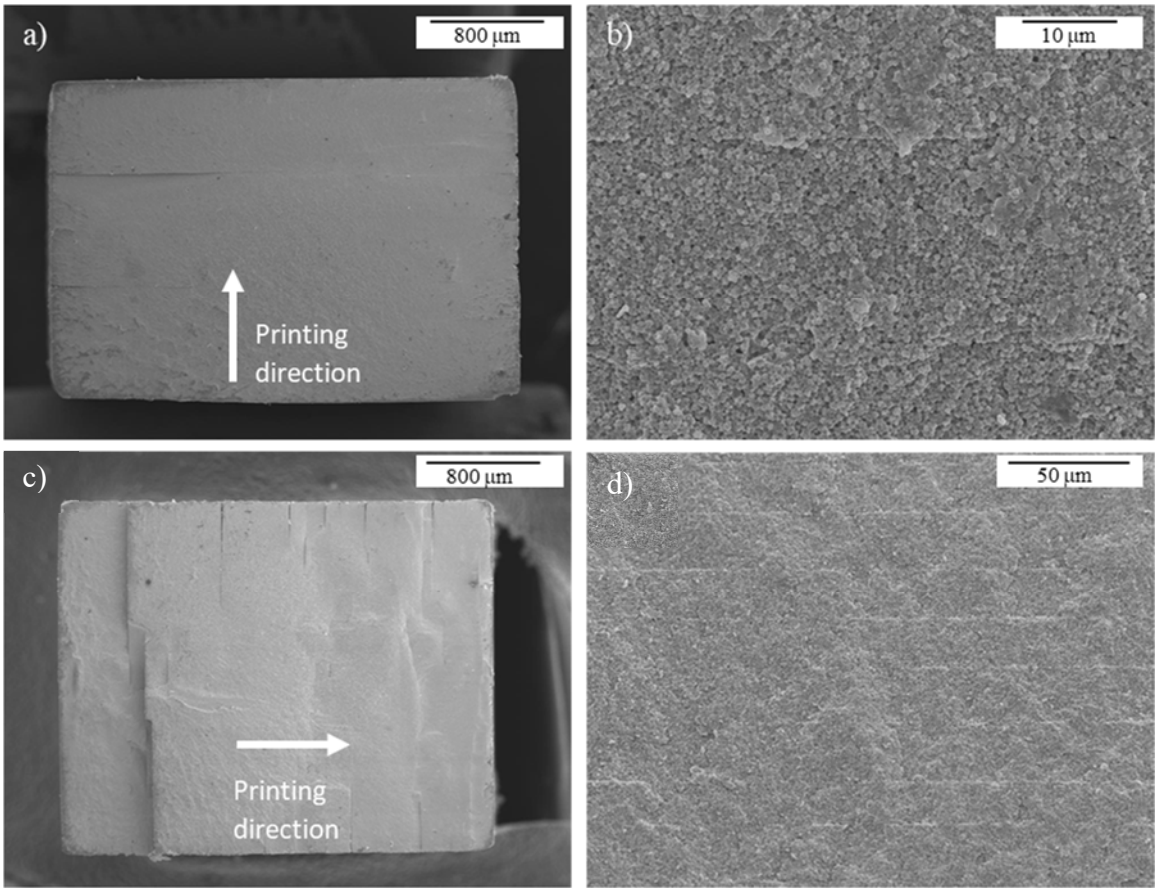

Figure 13: Fracture surface of the 81 wt% samples after flexural tests: XY (a,b) and XZ (c,d) printing directions. Images at lower (a,c) and higher (b,d) magnifications.

A previous study on the role of the printing direction on the mechanical properties was reported by Fu et al. [**30**], even if the layer-by-layer consolidation was performed through a UV laser in a SLA equipment. Authors obtained very high bending strength values (1044 MPa as average) when the loading direction was

perpendicular to the laser scanned surface (similarly to our XZ configuration), no matter the laser power. On the contrary, in the other direction (XY configuration), a significantly lower bending strength was achieved (around 700 MPa) at low laser power, but increased almost linearly with the laser power, achieving ~ 1000 MPa. Thus, in this last optimized condition a limited difference in flexural strength depending on the printing direction was observed. The Authors suggested that – as cured width and depth expanded with the increase of the laser power - the bonding forces between adjacent layers were improved, and thus mechanical properties. Similarly, Marsico et al. [**20**] determined a similar strength for bars printed along these two directions (and precisely 657 ± 84 MPa for 0°A samples, which correspond to XZ direction, and 554 ± 68 MPa for 0°B samples which correspond to XY direction), still justifying the slightly lower strength of the second group on the ground of the layer line orientation which can provide potential defects at the tensile surface of the specimens. Finally, as evidenced in **Figure 12**, elastic modulus is approx. constant for all the investigated compositions, no matter the solid loading and printing direction, in agreement with a previous work [**20**].

Vickers hardness was measured for the two compositions on samples printed in the XY and XZ configuration. For each configuration and composition, hardness was measured on the surface parallel to the printing plane and perpendicular to the printing plane, and results are collected in **Table 3**. In fact, even if this basic property is generally isotropic and thus independent on the printing direction, a possible effect of the interlayers was investigated, as the dimension of the indentations was of the same order of magnitude of the interlayer space (**Figure 4**).

Table 3: Vickers hardness, H, of the sintered ceramics. Values with indices // correspond to measurements made along the printing plane surface, while ⊥ corresponds to measurements made on the surface perpendicular to the printing plane.

Composition	$H_{//}$ (GPa)	$H_{\perp}$ (GPa)
79 wt% XY	11.77 ± 0.22	12.26 ± 0.25
79 wt% XZ	12.35 ± 0.16	12.34 ± 0.30
81 wt% XY	12.32 ± 0.23	12.18 ± 0.23
81 wt% XZ	12.34 ± 0.29	12.00 ± 0.55

No significant variation of Hardness with both the surface studied and the printing configuration were observed, thus confirming that this property is not affected by the layers lines and possible interlayer flaws and values are in line with values expected for 3 mol% yttria-doped zirconia [**21**], especially values for CY3Z fabricated by traditional methods and provided by Saint-Gobain (i.e. H=1250 Hv or 12.25 GPa). After mechanical testing, XRD analysis on the fracture surface (**Figure 7**) revealed that tetragonal zirconia only partially transformed into monoclinic (13%), being such limited zirconia transformation imputable to its ultrafine microstructure.

4. Conclusions

High solid loading zirconia slurries were successfully prepared and printed by DLP additive manufacturing. In particular, two solid loadings (40.5 and 43.6 vol%, respectively) and two different printing directions were investigated. After sintering 1h at 1550 °C both the formulations achieved a very high relative density (> 99.2 %TD) independently from the solid loading and printing direction, attesting the possibility to obtain ceramic parts with densities close to ceramics shaped through traditional techniques. FE-SEM micrographs revealed a fully dense microstructure with the typical fine grained microstructure of yttria-stabilized zirconia with an average grains size of 0.56 ± 0.19 μm. Indeed, no differences were recognized among the two investigated compositions nor the two printing directions. At the same time, the mechanical properties were just slightly influenced by printing direction and zirconia vol%. Samples were characterized in their as-sintered state, and those tested perpendicular to the printing plane showed higher flexural strength than samples tested parallel to the printing plane. In particular, the composition with the higher solid loading (i.e. 43.6 vol%) showed the highest three-point flexural strength (751 ± 83 MPa) when tested perpendicular to the printing plane. On the other side, elastic modulus and Vickers Hardness were not dependent on the printing direction, and showed values comparable to those of materials manufactured under conventional technologies. These promising results demonstrated that DLP technique is a viable solution to produce ceramic parts not only with properties comparable to traditionally shaped ceramics but also to avoid time consuming machining and post-processing. Finally, even if a certain anisotropy of the flexural strength can be recognized, the difference in values determined for XZ and XY samples always felt into the standard

deviation of the average values, thus suggesting that – once optimized both slurry and printing parameters – the layer lines played a minor role on the strength. In our case, just some cracks at the samples border were recognized, the minimization of which will be the subject of future works.

Declaration of Competing Interest

The authors declare that they have no known competing financial interests or personal relationships that could have appeared to influence the work reported in this paper.

Acknowledgments

The researches leading to these results have received funding from the European project AMITIE (Marie Skłodowska Curie Grant Agreement n°734342).

REFERENCES

[1] Chen, Z., Li, Z., Li, J., Liu, C., Lao, C., Fu, Y., Liu, C., Li, Y., Wang, P., He, Y. (2019). 3D printing of ceramics: A review. Journal of the European Ceramic Society, 39, 661-687. https://doi.org/10.1016/j.jeurceramsoc.2018.11.013

[2] Zhang, X., Wu, X., & Shi, J. (2020). Additive manufacturing of zirconia ceramics: a state-of-the-art review. *Journal of Materials Research and Technology*, *9* (4), 9029-9048. https://doi.org/10.1016/j.jmrt.2020.05.131

[3] Lian, Q., Wu, X., Li, D., He, X., Meng, J., Liu, X., & Jin, Z. (2019). Accurate printing of a zirconia molar crown bridge using three-part auxiliary supports and ceramic mask projection stereolithography. *Ceramics International*, *45* (15), 18814-18822. https://doi.org/10.1016/j.ceramint.2019.06.111

[4] Osman, R. B., van der Veen, A. J., Huiberts, D., Wismeijer, D., & Alharbi, N. (2017). 3D-printing zirconia implants; a dream or a reality? An in-vitro study evaluating the dimensional accuracy, surface topography and mechanical properties of printed zirconia implant and discs. *Journal of the mechanical behavior of biomedical materials*, *75*, 521-528. https://doi.org/10.1016/j.jmbbm.2017.08.018

[5] Xing, B., Cao, C., Zhao, W., Shen, M., Wang, C., & Zhao, Z. (2020). Dense 8 mol% yttria-stabilized zirconia electrolyte by DLP stereolithography. *Journal of the European Ceramic Society*, *40*(4), 1418-1423. https://doi.org/10.1016/j.jeurceramsoc.2019.09.045

[6] Takahashi, M., & Kirihara, S. (2021). Stereolithographic Additive Manufacturing of Zirconia Electrodes with Dendritic Patterns for Aluminum Smelting. *Applied Sciences*, *11*(17), 8168. https://doi.org/10.3390/app11178168

[7] Zhang, J., Wei, L., Meng, X., Yu, F., Yang, N., & Liu, S. (2020). Digital light processing-stereolithography three-dimensional printing of yttria-stabilized zirconia. *Ceramics International*, *46*(7), 8745-8753. https://doi.org/10.1016/j.ceramint.2019.12.113

[8] He, R., Liu, W., Wu, Z., An, D., Huang, M., Wu, H., ... & Xie, Z. (2018). Fabrication of complex-shaped zirconia ceramic parts via a DLP-stereolithography-based 3D printing method. Ceramics International, 44(3), 3412-3416. https://doi.org/10.1016/j.ceramint.2017.11.135

[9] Wang, L., Liu, X., Wang, G., Tang, W., Li, S., Duan, W., & Dou, R. (2020). Partially stabilized zirconia moulds fabricated by stereolithographic additive manufacturing via digital light processing. *Materials Science and Engineering: A*, *770*, 138537. https://doi.org/10.1016/j.msea.2019.138537

[10] Wang, J. C., & Dommati, H. (2018). Fabrication of zirconia ceramic parts by using solvent-based slurry stereolithography and sintering. The International Journal of Advanced Manufacturing Technology, 98(5-8), 1537-1546. https://doi.org/10.1007/s00170-018-2349-3

[11] Li, X., Zhong, H., Zhang, J., Duan, Y., Bai, H., Li, J., & Jiang, D. (2020). Dispersion and properties of zirconia suspensions for stereolithography. International Journal of Applied Ceramic Technology, 17(1), 239-247. https://doi.org/10.1111/ijac.13321

[12] Sun, J., Binner, J., & Bai, J. (2020). 3D printing of zirconia via digital light processing: optimization of the slurry and debinding process. Journal of the European Ceramic Society. https://doi.org/10.1016/j.jeurceramsoc.2020.05.079

[13] Zhang, K., He, R., Xie, C., Wang, G., Ding, G., Wang, M., ... & Fang, D. (2019). Photosensitive ZrO_2 suspensions for stereolithography. Ceramics International, 45(9), 12189-12195. https://doi.org/10.1016/j.ceramint.2019.03.123

[14] Li, X.-B., Zhong, H., Zhang, J.-X., Duan, Y.-S., & Jiang, D.-L. (2020). Powder Characteristics on the Rheological Performance of Resin-based Zirconia Suspension for Stereolithography. Journal of Inorganic Materials, 35 (2) 231-235. https://doi.org/10.1111/ijac.13321

[15] Borlaf, M., Serra-Capdevila, A., Colominas, C., & Graule, T. (2019). Development of UV-curable ZrO_2 slurries for additive manufacturing (LCM-DLP) technology. Journal of the European Ceramic Society, 39(13), 3797-3803. https://doi.org/10.1016/j.jeurceramsoc.2019.05.023

[16] Jang, K. J., Kang, J. H., Fisher, J. G., & Park, S. W. (2019). Effect of the volume fraction of zirconia suspensions on the microstructure and physical properties of products produced by additive manufacturing. Dental Materials, 35(5), e97-e106. https://doi.org/10.1016/j.dental.2019.02.001

[17] Ji, S.H., Da, S.K., Park, M.S., Ji, S.Y. (2021). Sintering Process Optimization for 3YSZ Ceramic 3D-Printed Objects Manufactured by Stereolithography. Nanomaterials, 11, 192-204. https://doi.org/10.3390/nano11010192

[18] Lu, Y., Mei, Z., Zhang, J., Gao, S., Yang, X., Dong, B., ... & Yu, H. (2020). Flexural strength and Weibull analysis of Y-TZP fabricated by stereolithographic additive manufacturing and subtractive manufacturing. Journal of the European Ceramic Society, 40(3), 826-834. https://doi.org/10.1016/j.jeurceramsoc.2019.10.058

[19] Harrer, W., Schwentenwein, M., Lube, T., Danzer, R. (2017) Fractography of zirconia-specimens made using additive manufacturing (LCM) technology. Journal of the European Ceramic Society, 37, 4331-4338. https://doi.org/10.1016/j.jeurceramsoc.2017.03.018

[20] Marsico, C., Øilob, M., Kutsch, J., Kauf, M., Arola, D. (2020). Vat polymerization-printed partially stabilized zirconia: Mechanical properties, reliability and structural defects. Additive Manufacturing 36, 101450, https://doi.org/10.1016/j.addma.2020.101450.

[21] https://www.zirpro.com/zirconia-beads-powders/3-mol-yttria-stabilized-zirconia (Accessed Oct. 2021)

[22] Coppola, B., Lacondemine, T., Tardivat, C., Montanaro, L., Palmero, P. (2021). Designing alumina-zirconia composites by DLP-based stereolithography: Microstructural tailoring and mechanical performances. Ceramics International, 47 (2021), 13457-13468. https://doi.org/10.1016/j.ceramint.2021.01.204

[23] Garvie, R.C., Nicholson, P.S. (2006). Phase Analysis in Zirconia Systems. Journal of the American Ceramic Society 55(6), 303 – 305. https://doi.10.1111/j.1151-2916.1972.tb11290.x

[24] Quinn, G. D., Patel, P. J., Lloyd, I. Effect of Loading Rate Upon Conventional Ceramic Microindentation Hardness. Journal of research of the National Institute of Standards and Technology, 107 (2002), 299–306. https://doi.org/10.6028/jres.107.023

[25] Licciulli, A., Corcione, C. E., Greco, A., Amicarelli, V., & Maffezzoli, A. (2005). Laser stereolithography of ZrO_2 toughened Al_2O_3. Journal of the European Ceramic Society, 25(9), 1581-1589. https://doi.org/10.1016/j.jeurceramsoc.2003.12.003

[26] Li, H., Liu, Y., Liu, Y., Zeng, Q., Hu, K., Lu, Z., Liang, J., & Li, J. (2021). Influence of debinding holding time on mechanical properties of 3D-printed alumina ceramic cores. Ceramics International, 47(4), 4884-4894. https://doi.org/10.1016/j.ceramint.2020.10.061

[27] K. Zhang, He, R., Ding, G., Feng, C., Song, W., Fang, D. (2020). Digital light processing of 3Y-TZP strengthened ZrO_2 ceramics. Materials Science & Engineering A 774, 138768. https://doi.org/10.1016/j.msea.2019.138768

[28] Fu, X., Zou, B., Xing, H., Li, L., Li, Y., & Wang, X. (2019). Effect of printing strategies on forming accuracy and mechanical properties of ZrO2 parts fabricated by SLA technology. Ceramics International, 45(14), 17630-17637. https://doi.org/10.1016/j.ceramint.2019.05.328